Supplementary Information for

Prediction of *p*-block-based ternary superconductors XC_2H_8 at low pressure

Izabela A. Wrona,[1] Paweł Niegodajew,[2] Yinwei Li,[3] and Artur P. Durajski[1,*]

[1] *Institute of Physics, Czestochowa University of Technology, Ave. Armii Krajowej 19, 42-200 Czestochowa, Poland*

[2] *Department of Thermal Machinery, Czestochowa University of Technology, Ave. Armii Krajowej 21, 42-200 Czestochowa, Poland*

[3] *Laboratory of Quantum Materials Design and Application, School of Physics and Electronic Engineering, Jiangsu Normal University, Xuzhou 221116, China*

(Dated: October 25, 2024)

The Supporting Information includes comprehensive data on the calculated electronic band structures, electronic localization functions (ELF), and phonon spectra for all energetically most favorable structures at 60 GPa. These details provide crucial insights into the electronic and vibrational properties of the materials under moderate-pressure conditions. In addition to the electronic and phononic characteristics, the Supporting Information offers a thorough explanation of the methodology used to calculate the critical temperature T_c. This calculation employs both the McMillan and Allen-Dynes equations, which are pivotal in understanding the superconducting properties of the materials. The derivations, assumptions, and parameters used in these calculations are meticulously documented to ensure reproducibility and to facilitate a deeper understanding of the factors influencing T_c.

Contents

* artur.durajski@pcz.pl

1. Crystal structure of $Fm\bar{3}m$-XC_2H_8

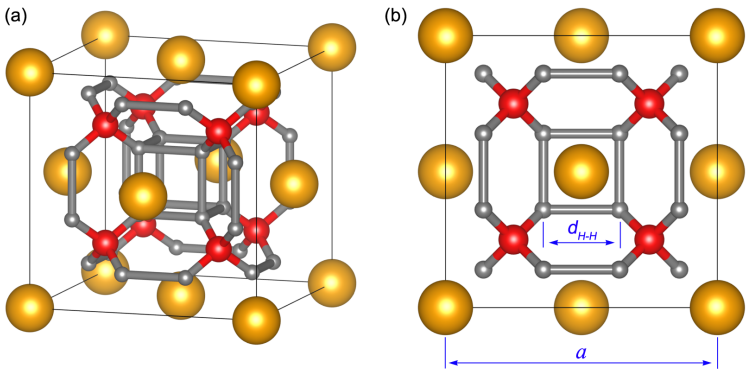

Supplementary Figure 1. **Crystal structure of $Fm\bar{3}m$-XC_2H_8.** Overall view (a) and side view (b) of the crystal structure of $Fm\bar{3}m$-XC_2H_8 with marked lattice parameter (a) and distance between hydrogen atoms (d_{H-H}). X, C, and H atoms are indicated as large orange, medium red, and small grey spheres, respectively.

2. Electronic band structures of $Fm\bar{3}m$-XC_2H_8 (X = Ga, In, Tl, Sn, Pb, Sb, Bi, Te, Po)

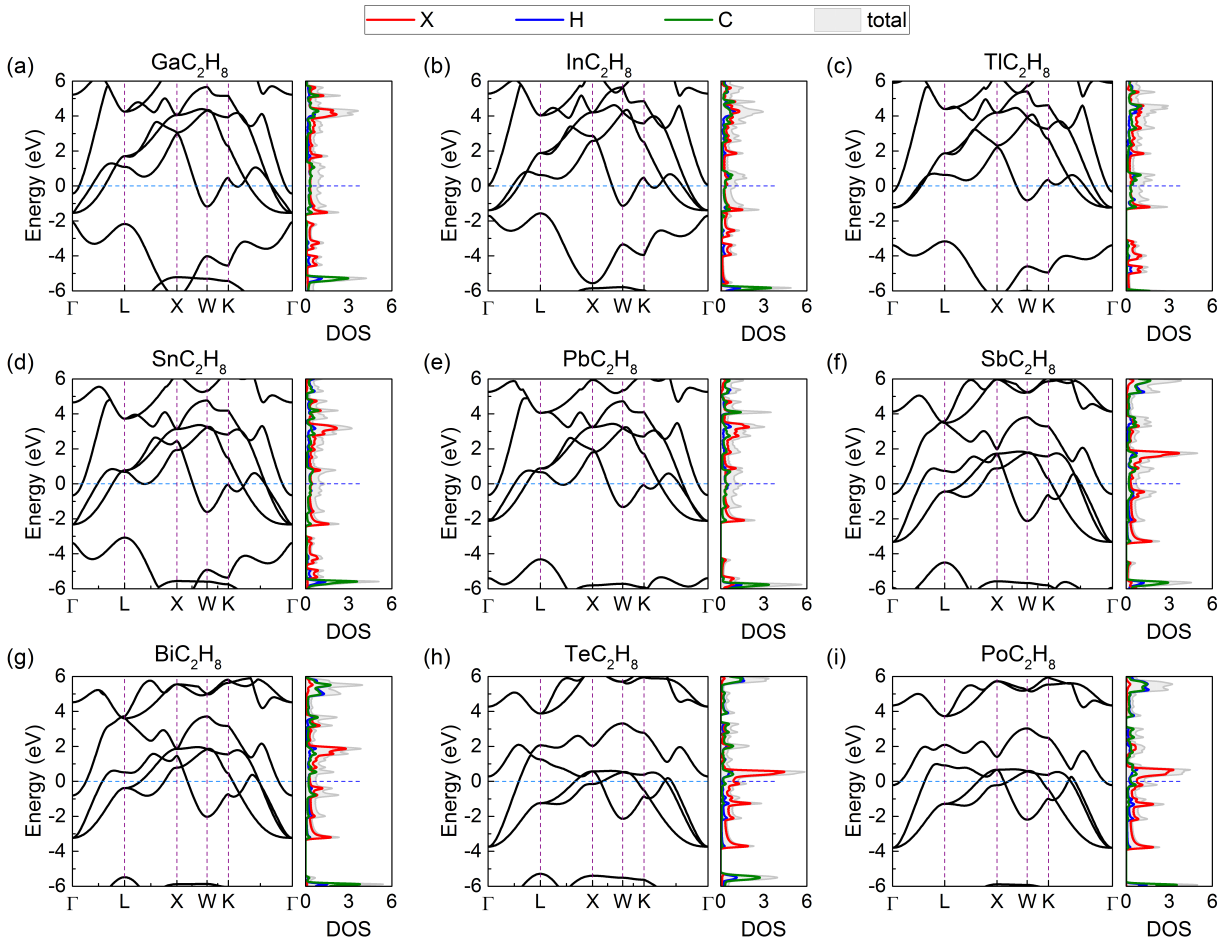

Supplementary Figure 2. **Electronic band structures of $Fm\bar{3}m$-XC_2H_8.** Electronic band structures and partial density of states (DOS, in states/eV) for (a) GaC_2H_8, (b) InC_2H_8, (c) TlC_2H_8, (d) SnC_2H_8, (e) PbC_2H_8, (f) SbC_2H_8, (g) BiC_2H_8, (h) TeC_2H_8, and (i) PoC_2H_8 at 60 GPa.

Supplementary Figure 3 presents a comparison of the electronic band structures for SbC_2H_8 calculated using different pseudopotentials. The comparison covers various pseudopotentials based on of PBE and PZ functionals, specifically: pbe-rrkjus (black solid line), pbe-kjpaw (blue solid line), pbe-hgh (orange solid line), pz-rrkjus (green dash-dotted line), pz-kjpaw (red dash-dotted line), pz-hgh (gray dash-dotted line). These pseudopotentials are classified according to two main criteria: the exchange-correlation functional used (PBE and PZ) and the type of pseudopotential method employed (rrkjus, kjpaw, hgh). In particular, PBE (Perdew-Burke-Ernzerhof functional) refers to the Generalized Gradient Approximation (GGA), commonly used for predicting accurate lattice constants, band gaps, and surface properties in various systems. PZ (Perdew-Zunger) refers to the Local Density Approximation (LDA) functional, often used for simpler and computationally efficient calculations, though it may underestimate certain properties, such as band gaps. The selection of pseudopotential plays a crucial role, not only contributing to the overall accuracy of the simulations but also significantly impacting the computational efficiency, determining how quickly and effectively the calculations can be performed. In particular, rrkjus refers to the norm-conserving pseudopotentials developed by Rappe, Rabe, Kaxiras, and Joannopoulos (RRKJ), which ensure norm conservation of the wavefunctions, making them more reliable for total energy and force calculations. The kjpaw (Kresse-Joubert projector-augmented wave) pseudopotentials are all-electron-like potentials that can model core and valence electrons more accurately, especially in the context of systems with transition metals or heavy elements. The hgh (Hartwigsen-Goedecker-Hutter) pseudopotentials are ultra-soft and optimized for efficiency, useful in cases where computational resources are a constraint. In Fig. 3, the bands from the various pseudopotentials are closely aligned, indicating

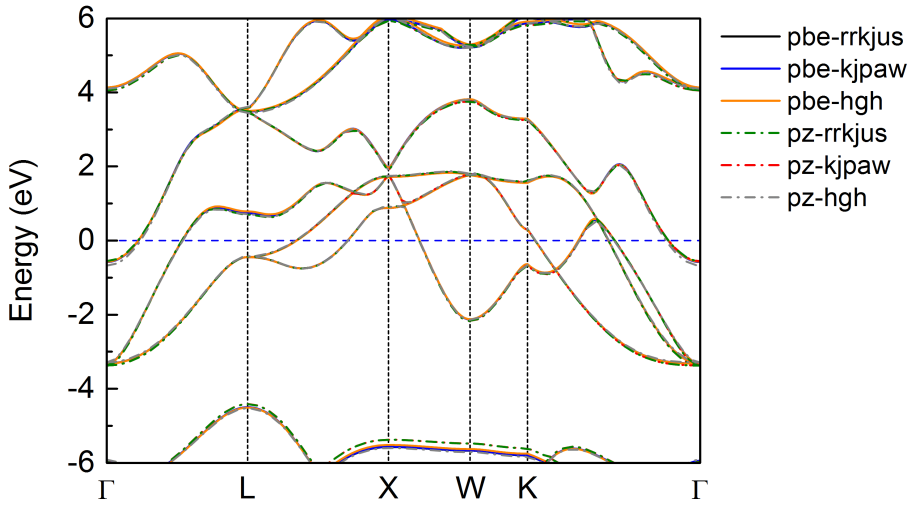

Supplementary Figure 3. **Comparison of electronic band structure for SbC_2H_8.** Comparison of electronic band structure for SbC_2H_8 at 60 GPa calculated for different pseudopotentials.

that all pseudopotentials yield consistent predictions of the electronic structure. This close agreement, especially near the Fermi level, demonstrates the reliability of the chosen pbe-rrkjus pseudopotentials for studying SbC_2H_8 and other XC_2H_8 systems under compression. Despite minor variations in the deeper energy bands, the overall metallic character is well captured by each pseudopotential. This comparison helps in evaluating the robustness of the computational results, ensuring that the choice of pseudopotential has minimal impact on the conclusions drawn from the band structure analysis.

3. Electronic localization function of $Fm\bar{3}m$-XC_2H_8 (X = Ga, In, Tl, Sn, Pb, Sb, Bi, Te, Po)

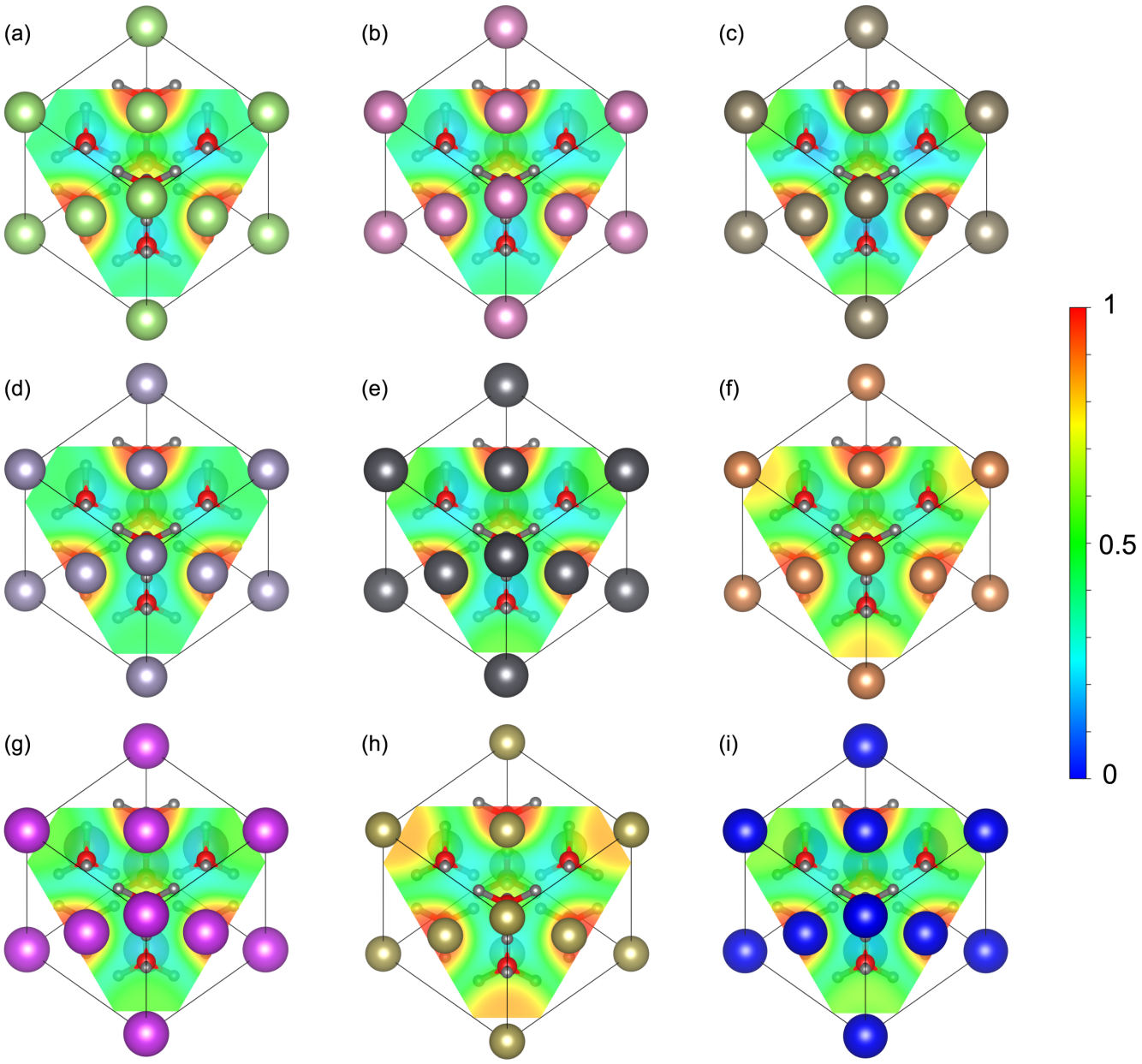

Supplementary Figure 4. **Electronic localization function of $Fm\bar{3}m$-XC_2H_8.** Electronic localization function (ELF) for (a) GaC_2H_8, (b) InC_2H_8, (c) TlC_2H_8, (d) SnC_2H_8, (e) PbC_2H_8, (f) SbC_2H_8, (g) BiC_2H_8, (h) TeC_2H_8, and (i) PoC_2H_8 at 60 GPa.

4. Phonon dispersion and phonon density of states for $Fm\bar{3}m$-XC_2H_8 (X = Ga, In, Tl, Sn, Pb, Sb, Bi, Te, Po)

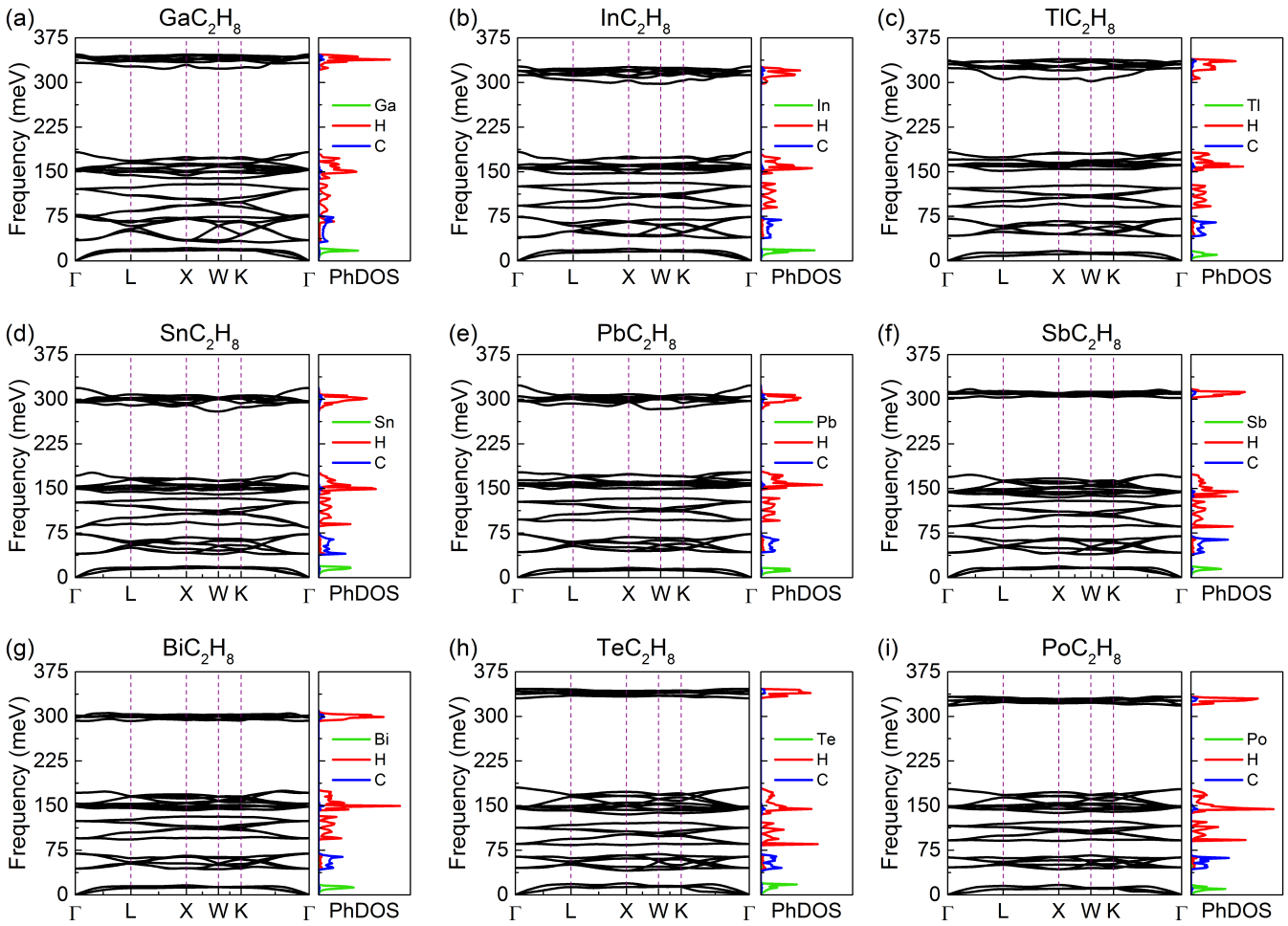

Supplementary Figure 5. **Phonon dispersion and phonon density of states for $Fm\bar{3}m$-XC_2H_8.** The calculated phonon dispersion and projected phonon density of states for (a) GaC_2H_8, (b) InC_2H_8, (c) TlC_2H_8, (d) SnC_2H_8, (e) PbC_2H_8, (f) SbC_2H_8, (g) BiC_2H_8, (h) TeC_2H_8, and (i) PoC_2H_8 at 60 GPa.

5. Eliashberg functions and EPC coefficients for $Fm\bar{3}m$-XC_2H_8 (X = Ga, In, Tl, Sn, Pb, Sb, Bi, Te, Po)

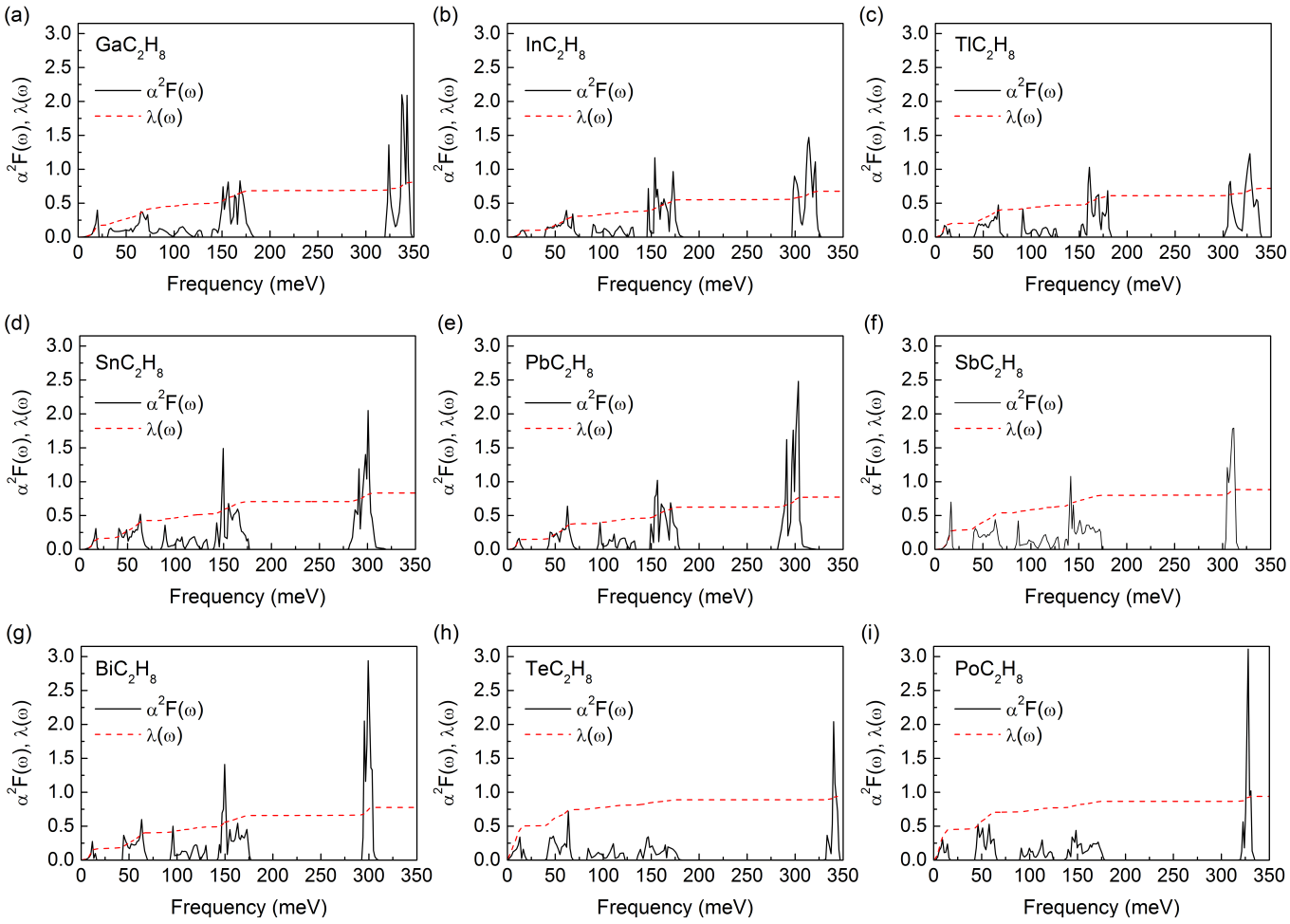

Supplementary Figure 6. **Eliashberg functions and EPC coefficients.** Eliashberg spectral functions and EPC coefficients for (a) GaC_2H_8, (b) InC_2H_8, (c) TlC_2H_8, (d) SnC_2H_8, (e) PbC_2H_8, (f) SbC_2H_8, (g) BiC_2H_8, (h) TeC_2H_8, and (i) PoC_2H_8 at 60 GPa.

6. Critical temperature for $Fm\bar{3}m$-XC_2H_8 (X = Ga, In, Tl, Sn, Pb, Sb, Bi, Te, Po)

Besides the Eliashberg approach, described in the main text, the critical temperature (T_c) can be also calculated using the Allen-Dynes formula [1–4]:

$$k_B T_C = \frac{f_1 f_2 \omega_{\log}}{1.20} \exp\left(-\frac{1.04\,(1+\lambda)}{\lambda - \mu^\star - 0.62\lambda\mu^\star}\right), \tag{1}$$

where $\omega_{\log}$, λ and μ^* denote logarithmic average phonon frequency, the electron-phonon coupling constant and Coulomb pseudopotential ($\mu^\star = 0.1$ and 0.15), respectively. Logarithmic phonon frequency and electron-phonon coupling constant are given as:

$$\omega_{\log} = \exp\left(\frac{2}{\lambda}\int_0^{\omega_{\max}} \mathrm{d}\omega \frac{\alpha^2 F(\omega)\ln(\omega)}{\omega}\right) \tag{2}$$

and

$$\lambda = 2\int_0^{\omega_{\max}} \frac{\alpha^2 F(\omega)}{\omega}\mathrm{d}\omega. \tag{3}$$

Additionally, $f_1 f_2$ is the correction factor introduced by Allen and Dynes, which can be defined as [3, 4]:

$$f_1 f_2 = \left[1 + \left(\frac{\lambda}{2.46(1+3.8\mu^*)}\right)^{3/2}\right]^{1/3} \left[1 + \frac{\left(\frac{\sqrt{\omega_2}}{\omega_{\log}} - 1\right)\lambda^2}{\lambda^2 + \left(1.82\,(1+6.3\mu^\star)\left(\frac{\sqrt{\omega_2}}{\omega_{\log}}\right)\right)^2}\right]. \tag{4}$$

In the equations above ω_2 is the second moment of the normalized weight function which can be calculated from the expression $\omega_2 = \frac{2}{\lambda}\int_0^{\omega_{\max}} \mathrm{d}\omega\alpha^2 F(\omega)\omega$. The McMillan approach assumes that $f_1 f_2 = 1$ [1]. The correction in the Allen-Dynes formula has been intended to adapt the McMillan equation to the cases with strong electron-phonon coupling. A modification to the correction factor, which offers a more precise characterization of the superconducting transition temperature, is presented as follows [5, 6]:

$$f_1 f_2 = \left[1 + \left(\frac{\lambda}{2.46(1+3.8\mu^*)}\right)^{3/2}\right]^{1/3} \left[1 + \frac{\left(\frac{\sqrt{\omega_2}}{\omega_{\log}} - 1\right)\lambda^2}{\lambda^2 + \left(1.82\,(1+6.3\mu^\star)\right)^2}\right]. \tag{5}$$

This refinement demonstrates improved agreement with results obtained from direct solutions of the Eliashberg equations, offering a more reliable prediction of the high transition temperature compared to previous approaches. The T_c values calculated using these three analytical approaches are compared in Supplementary Table I with the results obtained from the Eliashberg equations. Moreover, Supplementary Fig. 7 shows the correlation between the transition temperature solved from the Eliashberg approach (Eqs (4) and (5) from the main text) and various models, i.e. McM (McMillan, Eq. 1 with $f_1 f_2 = 1$), AD (original Allen-Dynes, Eq. 1 with Eq. 4) and AD-corr (corrected Allen-Dynes, Eq. 1 with Eq. 5).

In addition, Fig. 8 presents the pressure dependence of the superconducting critical temperature and temperature dependence of the superconducting energy gap at 60 GPa for $Fm\bar{3}m$-XC_2H_8 (X = Ga, In, Tl, Sn, Pb, Sb, Bi, Te, Po). Herein we have taken into account only the dynamical stability criterion for $Fm\bar{3}m$ crystal structure (the enthalpy minimization criterion is neglected).

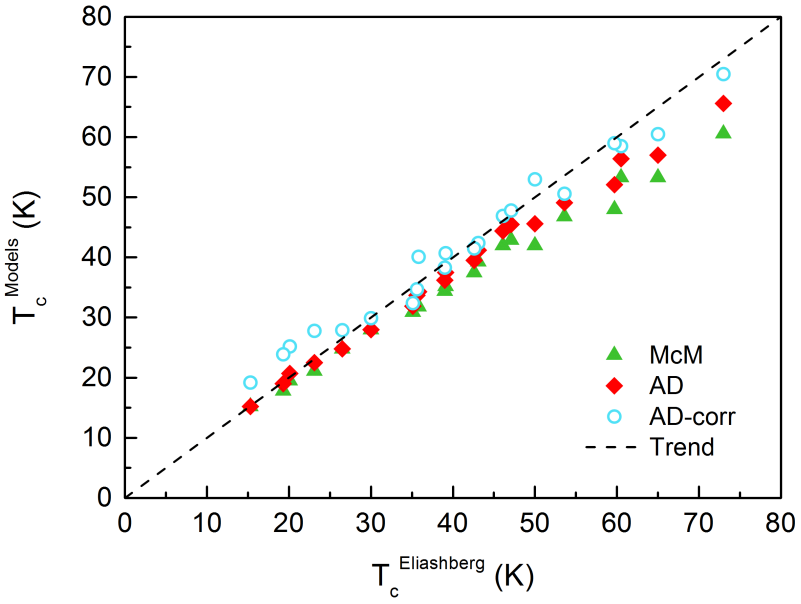

Supplementary Figure 7. The correlation between the superconducting transition temperature calculated using the Eliashberg approach and various theoretical models: McM (McMillan equation, green triangles), AD (original Allen-Dynes equation, red diamonds), and AD-corr (corrected Allen-Dynes equation, blue circles). The black dashed trend line represents a perfect correlation.

Supplementary Table I. Predicted superconducting properties of $Fm\bar{3}m$-XC_2H_8 ternary hydrides. In particular, pressure (p, in GPa), the electron-phonon coupling constant (λ), logarithmic average phonon frequency ($\omega_{\log}$), second moment of the normalized weight function (ω_2), superconducting transition temperature calculated for $\mu^\star = 0.1$ (0.15) using McMillan ($T_c^{\rm McM}$), Allen-Dynes ($T_c^{\rm AD}$), corrected Allen-Dynes ($T_c^{\rm AD}$-corr) and Eliashberg ($T_c^{\rm E}$) equations are listed.

parameter	p	GaC_2H_8	InC_2H_8	TlC_2H_8	SnC_2H_8	PbC_2H_8	SbC_2H_8	BiC_2H_8	TeC_2H_8	PoC_2H_8
λ	20	1.00	0.89	0.82	-	-	-	-	-	-
	60	0.81	0.68	0.72	0.83	0.77	0.88	0.78	0.94	0.94
	100	0.73	0.60	0.63	0.83	0.75	1.02	0.91	1.06	1.05
$\omega_{\log}$ (K)	20	459	340	311	-	-	-	-	-	-
	60	878	1010	668	846	865	621	780	282	335
	100	1044	1331	1059	1045	1151	843	887	557	646
$\sqrt{\omega_2}$ (K)	20	1360	1310	1285	-	-	-	-	-	-
	60	1850	1907	1766	1684	1828	1448	1703	1155	1294
	100	1894	2087	2059	1045	2061	1674	1780	1526	1610
$T_c^{\rm McM}$ (K)	20	31.8 (24.4)	19.5 (14.3)	15.2 (10.6)	-	-	-	-	-	-
	60	42.0 (29.1)	32.3 (19.6)	24.8 (15.8)	42.9 (30.2)	37.5 (25.2)	35.2 (25.6)	34.4 (23.2)	17.8 (13.3)	21.1 (15.8)
	100	39.3 (25.3)	30.9 (16.6)	28.0 (15.9)	53.3 (37.6)	46.8 (30.8)	60.6 (46.9)	53.3 (39.3)	42.0 (32.8)	48.0 (37.4)
$T_c^{\rm AD}$ (K)	20	34.3 (25.9)	20.7 (14.9)	15.9 (11.0)	-	-	-	-	-	-
	60	44.4 (30.4)	33.7 (20.3)	25.9 (16.4)	45.5 (31.6)	39.5 (26.2)	37.5 (26.9)	36.2 (24.2)	19.0 (14.0)	22.5 (16.6)
	100	41.2 (26.2)	31.9 (17.1)	29.1 (16.4)	56.4 (39.3)	49.1 (32.0)	65.6 (49.9)	57.0 (41.5)	45.6 (35.0)	52.1 (39.9)
$T_c^{\rm AD}$-corr (K)	20	40.1 (29.1)	25.2 (17.3)	19.2 (12.6)	-	-	-	-	-	-
	60	46.9 (31.7)	34.7 (20.7)	27.9 (17.3)	47.8 (32.8)	41.5 (27.2)	40.7 (28.6)	38.3 (25.2)	23.9 (16.6)	27.8 (19.5)
	100	42.4 (26.8)	32.4 (17.2)	29.9 (16.7)	58.5 (40.4)	50.6 (32.7)	70.5 (52.6)	60.5 (43.4)	53.0 (39.2)	59.0 (43.8)
$T_c^{\rm E}$ (K)	20	35.8 (29.5)	20.1 (16.2)	15.3 (12.0)	-	-	-	-	-	-
	60	46.1 (36.0)	35.6 (26.7)	26.5 (19.0)	47.1 (37.7)	42.6 (32.1)	39.1 (31.4)	39.0 (30.1)	19.3 (15.8)	23.1 (18.4)
	100	43.1 (33.5)	35.1 (25.0)	30.0 (21.8)	60.5 (48.1)	53.6 (41.1)	73.0 (60.7)	65.0 (52.1)	50.0 (41.6)	59.7 (48.1)

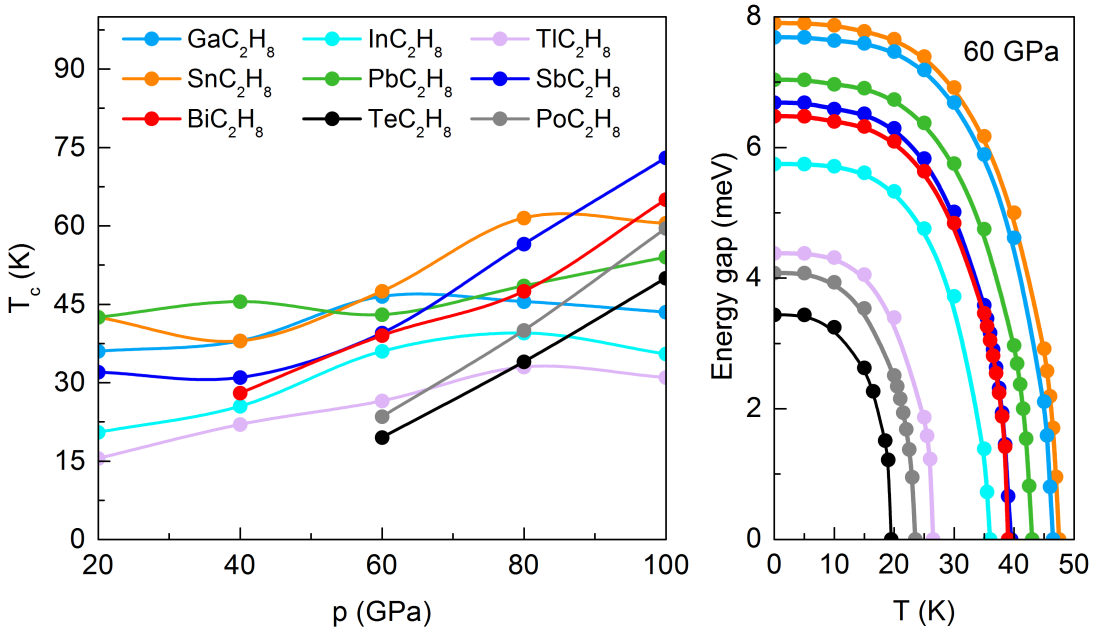

Supplementary Figure 8. **Critical temperature and superconducting energy gap.** Critical temperature and superconducting energy gap for GaC_2H_8, InC_2H_8, TlC_2H_8, SnC_2H_8, PbC_2H_8, SbC_2H_8, BiC_2H_8, TeC_2H_8, PoC_2H_8 in dynamically stable $Fm\bar{3}m$ structure obtained using Migdal-Eliashberg approach.

7. Relative enthalpies for AlC_2H_8, SiC_2H_8, GeC_2H_8, AsC_2H_8

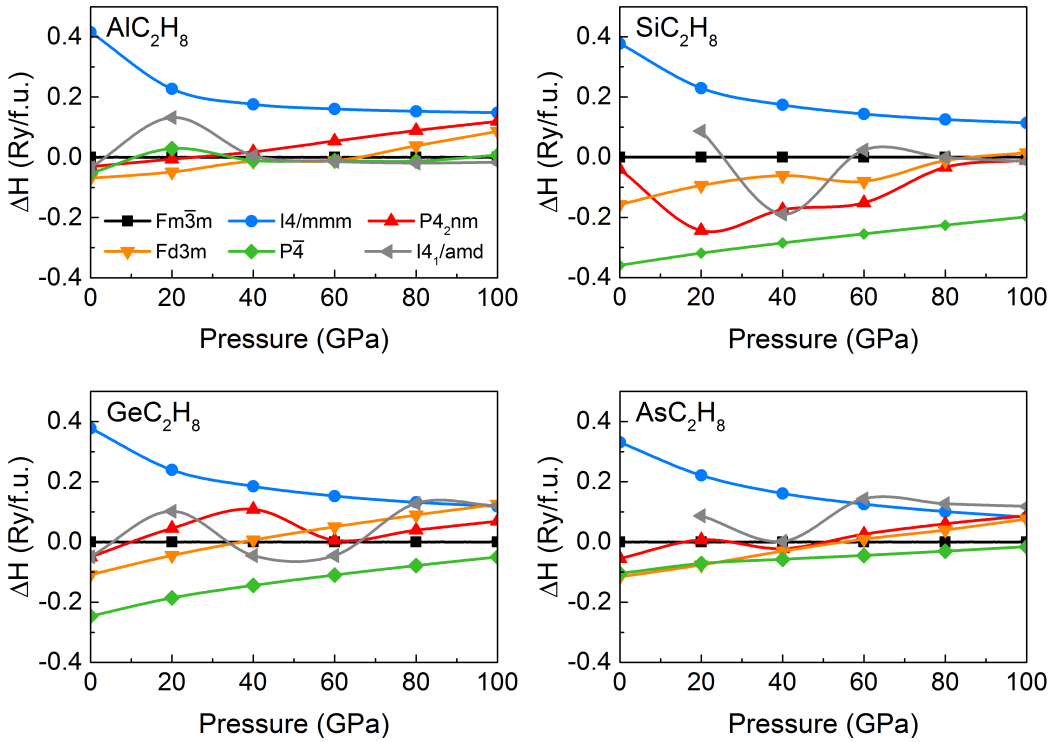

Supplementary Figure 9. **Relative enthalpies.** Relative enthalpies for AlC_2H_8, SiC_2H_8, GeC_2H_8, AsC_2H_8.

[1] W. L. McMillan, "Transition temperature of strong-coupled superconductors," Physical Review **167**, 331–344 (1968).
[2] R.C. Dynes, "McMillan's equation and the T_c of superconductors," Solid State Communications **10**, 615–618 (1972).
[3] P B Allen and R C Dynes, "Superconductivity at very strong coupling," Journal of Physics C: Solid State Physics **8**, L158 (1975).
[4] P. B. Allen and R. C. Dynes, "Transition temperature of strong-coupled superconductors reanalyzed," Physical Review B **12**, 905–922 (1975).
[5] Peng Song, Artur P. Durajski, Zhufeng Hou, Abdul Ghaffar, Rohit Dahule, Radosław Szczesniak, Kenta Hongo, and Ryo Maezono, "(La,Th)H_{10}: Potential high-T_c (242 K) superconductors stabilized thermodynamically below 200 GPa," The Journal of Physical Chemistry C **128**, 2656–2665 (2024).
[6] P. Song, Z. Hou, K. Nakano, K. Hongo, and R. Maezono, "Potential high-T_c superconductivity in $YCeH_x$ and $LaCeH_x$ under pressure," Materials Today Physics **28**, 100873 (2022).